Confined surface plasmon-polariton amplifiers

Stéphane Kéna-Cohen†, Paul N. Stavrinou, Donal D.C. Bradley and Stefan A. Maier

Department of Physics,

Imperial College London, London, SW7 2AZ

United Kingdom

†To whom correspondence should be addressed. E-mail: s.kena-cohen@imperial.ac.uk

Abstract

We demonstrate the realization of confined surface plasmon polariton amplifiers using a thin layer of the organic gain medium 4-dicyanomethylene-2-methyl-6-(p-dimethylaminostyryl)-4H-pyran dispersed in a tris(8-hydroxy-quinolinato)aluminum matrix. Complete loss compensation, which occurs at a pump fluence of approximately 200 μJ/cm^2, is directly observed in the time domain and studied for a range of waveguide lengths. The power dependence is also reported and a significant net gain of 93 dB/mm is observed at the highest fluence.

Keywords

Surface plasmons, waveguides, loss compensation, amplifiers, organic lasers, gain

Surface plasmon polaritons (SPPs) are surface excitations resulting from the coupling between collective electron oscillations, or plasmons, which occur in metals and highly doped semiconductors, with the electromagnetic waves in an adjoining dielectric.[1, 2] Their simplest implementation, which consists of a single-interface SPP, is transverse magnetic (TM) polarized and highly spatially confined due to the surface and electronic character of the excitation. The sub-wavelength confinement achieved using SPPs has garnered significant attention for use in small footprint optoelectronic components. Indeed, various waveguide and device geometries have been proposed, and implemented, to exploit the properties of SPPs.[3, 4] Their lossy character at optical frequencies, however, typically limits the propagation length to a few tens of wavelengths. In this work, we show that the loss of SPPs in a confined waveguide geometry can be completely compensated using an optically pumped gain medium and demonstrate net amplification of an SPP probe beam at pump fluences beyond 200 μJ/cm^2.

The first theoretical studies of the effect of gain on SPP absorption were performed more than thirty years ago,[5] yet it is only recently that convincing demonstrations of SPP amplification have been achieved.[6-8] These experiments relied on the amplification of long-range SPPs (LRSPPs), a mode specific to symmetric semi-infinite insulator-metal-insulator (IMI) structures that is characterized by extremely low losses. Their long propagation length is a consequence of high field delocalization within the dielectric medium.[9] Indeed, typical mode areas of LRSPP waveguides are much larger than λ^2, where λ is the free space wavelength, due to large modal extent in the direction perpendicular to the metal. Interestingly, one advantageous feature of LRSPP

amplifiers is their low noise figure resulting from reduced spontaneous emission into the LRSPP mode.[8, 10]

Net gain is also a prerequisite for the realization of spasers and nanolasers.[11] The former rely on overcoming the radiation and absorption losses of localized surface plasmons, thus triggering oscillation, while the latter rely on the amplification of SPPs confined within a resonator. Both types of lasers have recently been realized.[12-15] In particular, initial demonstrations of the latter have exploited hybrid plasmonic modes formed when a metal surface is separated from a dielectric by a low index gap region.[16] The resulting supermode allows the field intensity to be highly localized within the gap region, while keeping the losses moderately low. This approach has led to the demonstration of nanolasers with mode areas as low as $\lambda^2/400$. The nanorod and nanoflake waveguide geometries employed in such nanoscale light sources, however, greatly limit their usefulness as amplifiers or for interfacing with more complex plasmonic circuitry.

The direct observation of SPP amplification in confined waveguide geometries has, indeed, been elusive. There have been reports of partial loss-compensation in conventional SPP waveguides using colloidal PbS quantum dots (QDs) under continuous wave (CW) excitation,[17, 18] but the indirect nature of these measurements leaves them susceptible to artefacts arising from pump-induced fluorescence, thermo-optic effects and ground-state bleaching of the PbS absorption. In fact, to our knowledge, there has not as of yet been evidence of CW gain from colloidal QDs in dielectric waveguides and recent reports suggest that overcoming losses arising from Auger recombination may be a challenge.[19]

In this work, we report on the direct observation of plasmonic amplification in confined and lithographically defined SPP waveguides of varying length. At the highest pump powers, we find that the SPP loss is completely compensated by the optically pumped organic gain medium and results in a substantial net gain of 93 dB/mm for the best amplifier investigated. The waveguides used here possess a modest confinement corresponding to a mode area $A_m = 0.5\lambda^2$. As compared to previous reports on LRSPP amplifiers, losses one order of magnitude higher, concomitant with the higher confinement, can be compensated at pump fluences nearly one order of magnitude lower. The use of Au, as compared to silver, leads to higher losses, but Au has been the metal of choice for plasmonic circuitry due to its intrinsic stability.[3, 4] The gain medium used consists of the organic laser dye 4-dicyanomethylene-2-methyl-6-(p-dimethylaminostyryl)-4H-pyran (DCM) dispersed in a tris(8-hydroxy-quinolinato)aluminum (Alq$_3$) matrix.[20-23] This medium relies on Förster energy transfer from the wide optical gap host (Alq$_3$) to the narrow gap guest (DCM). As a result, ground state optical losses can be kept negligible due to the large spectral shift between the absorbing (host) and gain (guest) regions. The high absorbance of the host matrix allows gain to occur at lower fluence than in previous demonstrations. The absorbance, photoluminescence, which is representative of the spectral gain, and a typical amplified spontaneous emission (ASE) spectrum for Alq$_3$:DCM are shown in Fig. 1a. In organic solid-state lasers and transient absorption measurements, this material set has been demonstrated to possess gains in excess of 650 cm^{-1}.[21, 24] At our doping concentration of 1.5% v/v, the highest achievable gain in the absence of loss mechanisms is 10^4 cm^{-1} , obtained via the product of the number density of DCM molecules (3.7×10^{19} cm^{-3}) with

its emission cross-section (σ_e = 2.7 x 10^{-16} cm^2, see Supporting Information). In practice, however, several mechanisms contribute to reducing this value. It will be shown that the measured amplifier gain is consistent with modal calculations accounting for both the pump field distribution and the modified spontaneous emission lifetime.[25]

An optical micrograph of the fabricated waveguides is shown in Fig. 1b. The waveguide length is varied between 10 and 50 μm, in steps of 5 μm, while the width is kept fixed at 1 μm. The 21 nm-thick gold stripes are covered with 130 nm of Alq$_3$:DCM to provide optical gain. Note that such a thin organic layer does not support any guided modes when placed directly on the substrate. This is in strong contrast to previous demonstrations where thick active or cladding layers were used.[7, 8, 17, 18, 26] Here, the presence of the metal, and of the resulting SPP mode, is critical for achieving gain.

Input and output gratings were defined on the edge of each waveguide to in- and out-couple the probe signal at λ = 633 nm. Figure 1c shows images of a 50 μm-long waveguide when the probe beam is focused onto the input grating, for both TM and TE polarization. An output signal is clearly visible for the TM-polarized probe, while nothing is observed for TE-polarization. For all waveguide lengths investigated, only weak directly scattered light can be observed for TE-polarization, consistent with the TM nature of the propagating SPP-mode.

To measure the waveguide propagation length in the absence of the pump, the output signal intensity was measured for each fabricated length and this measurement was repeated for five independent sets of waveguides to avoid variations due to the position-dependence of the grating in-coupling efficiency. From a simple exponential fit to the data, shown in Fig. 2, a SPP propagation length of L_{exp} = (16.9 ± 0.7) μm is

extracted, corresponding to a power propagation loss of $\alpha_{exp} = (258 \pm 11)$ dB/mm. The inset shows the waveguide structure, overlaid on a finite element method (FEM) calculation of the investigated mode. An important point to note is that only two bound modes are supported by the structure and that they are purely plasmonic in nature (see Supporting Information). They are composed of the symmetric and anti-symmetric combinations of the single interface SPPs.[27] Calculations show that the symmetric mode possesses significantly lower loss ($n_{eff} = 1.540$, $L_{SPP} = 27.5$ μm, $A_m = \lambda^2/2$) than its anti-symmetric counterpart ($n_{eff} = 2.662$, $L_{SPP} = 0.2$ μm, $A_m = \lambda^2/32$). By using a Au thickness close to cutoff, the propagation length of this low-loss mode is improved over that of the semi-infinite Au/organic/air SPP ($n_{eff} = 1.870$, $L_{SPP} = 1.1$ μm, $A_m = \lambda^2/16$), but at the expense of confinement. The grating phase-matching condition is chosen to couple to this lower-loss guided mode, while the finite stripe width ensures that only a single transverse mode, which is the one shown in the inset, is supported for this combination (see Methods). The presence of a single transverse symmetric mode was found to be necessary to simplify the interpretation of the loss-compensation experiments. We have found, however, that in wider waveguides, multi-mode interference could be specifically exploited to create large modulations of the output in the presence of the pump.

The experimental setup used to perform the loss-compensation measurements is shown in Fig. 3a (see Methods for more details). The output from a λ=355 nm, Nd:YAG laser providing 1.8 ns-long pulses is shaped using a slit, before being focused onto the sample via a NA=0.42, 50X NUV objective resulting in a 67 μm x 10 μm rectangular stripe (Fig. 3b). The λ=633 nm, 2.5 mW, continuous wave (CW) probe beam is focussed from normal incidence onto the input grating of the waveguide being investigated, while

the output signal is spatially selected using an iris and collected using a fast PMT. Note that due to the high peak power of the pump, as compared to the CW probe, the broad fluorescence directly radiated from the collection region is much stronger than the signal output. To minimize this direct fluorescence contribution, only the optical power within a 1 nm bandwidth around the probe is collected.

A typical measurement showing the pump–probe signal for both TE and TM-polarized probe polarization as well as the pump-induced fluorescence is shown in Fig. 3c for a 30 µm long waveguide. Note that for guest-host systems such as Alq_3:DCM, the pump polarization is irrelevant since any polarization memory is lost after the Förster transfer process. It can be seen that since the waveguide only transmits TM-polarized light, the pump–probe (TE) and pump only signals are nearly identical. The peak around 20 ns, which is coincident with the arrival of the pump pulse, results solely from direct fluorescence emitted from the sample. The weak DC contribution to the signal present for the TE probe polarization corresponds to scattered input probe light which is collected by the PMT. On the other hand the strong TM-polarized DC contribution from the probe corresponds to light which propagates through the waveguide and is radiated *via* the output grating as shown in Fig. 1c. We find that, after subtracting the fluorescence and weak scatter from the raw data, the TM-polarized probe signal is increased by a factor F = 3.2 ± 0.1 in the presence of the pump. The 3.6 ns-long PMT instrument response function further reduces the measured peak amplitude (see Supporting Information) and after deconvolution we find that the gain is G = 7.1 ± 0.2, or equivalently (8.5 ± 0.2) dB. This gain just overcomes the SPP loss of -7.8 dB and corresponds to a material modal gain of 650 cm^{-1}, consistent with previous reports for gain in Alq_3:DCM.

To investigate the power dependence of the material gain, we have measured the signal enhancement as a function of the incident pump fluence for a 40 μm long waveguide and simultaneously recorded the fluorescence. From the results, shown in Fig. 3d, it is clear that the amplifier is operating well-within the saturation regime and that no significant pump depletion occurs due to the presence of the probe beam confirming that we are in the small-signal regime. The grey region corresponds to net gain. In conventional amplifiers saturation can occur due to ground-state depletion due to or to excited-state (pump) depletion due to amplified spontaneous emission (ASE).[28] For the SPP waveguide, ASE can only lead to significant field intensities beyond the net gain threshold, but we find that saturation happens at fluences well below this value. Indeed, it can be shown that at its local maximum, the exciton generation rate reaches values of 1×10^{28} cm^{-3}s^{-1} at a pump fluence of only 48 μJ/cm^2 (see Supporting Information). In the linear regime, this would correspond to a steady-state density of occupied DCM molecules of 2×10^{19} cm^{-3}, which is comparable to the DCM concentration. However, in contrast to the ground-state saturation typically observed for direct dye excitation, saturation here appears to result from bimolecular annihilation mechanisms which reduce the achievable inversion (see Supporting Information for a qualitative model).[29] This also differs from the situation typically observed in optically pumped organic lasers where saturation occurs due to depletion via stimulated emission.

All of the experiments were performed in ambient conditions, and as a result, photobleaching of the gain medium can be a concern at the highest pump intensities. We found that over time scales of a few minutes, a lowering of the fluorescence intensity could be observed at the highest pump fluence (503 μJ/cm^2). Even at this highest fluence,

however, no degradation was observed over the time scale of the experiment (10^3 pulses at 70 Hz). This is clearly seen, for example, in Fig. 3c, where the fluorescence intensity remains the same for the pump–probe (TE) and pump–only signals. Note that organic lasers based on Alq_3:DCM have previously demonstrated operational lifetimes of $>10^6$ pulses in ambient conditions, at pump fluences of 2 mJ/cm^2.[21]

To obtain reliable statistics on the loss-compensation in these waveguides, we have performed systematic measurements of the signal enhancement as a function of waveguide length for five independent sets of waveguides. The mean enhancement, standard deviation, maxima and minima are shown Figs. 4a and 4b for pump fluences of $F_p = 48$ µJ/cm^2 and $F_p = 200$ µJ/cm^2, respectively. The dashed line indicates the net gain threshold. It can be seen that a relatively large variation in the enhancement is observed, as compared to passive loss measurements (Fig. 2). This may be related to greater sensitivity to the conformal coating of the waveguides by the gain medium and to varying structural defects between the waveguides. We find that only a handful of measurements exceed the net gain threshold at $F_p = 48$ µJ/cm^2, but that net gain can be exceeded for all waveguide lengths, except 50 µm, at $F_p = 200$ µJ/cm^2. The slight drop observed for the 50 µm-long waveguide could be due to spatial variations in the pump profile (see Supporting Information). A linear fit to the $F_p = 200$ µJ/cm^2 data gives a signal enhancement of (261 ± 12) dB/mm, and a corresponding net signal gain of $g = (3.4 \pm 16)$ dB/mm. We see from Fig. 3d that no gain clamping occurs around this value and that further increases in pump power lead to higher gain, but with increased saturation.

A simple model was proposed by de Leon and Berini and extended to 2D by Colas des Francs *et al.* to account for quenching effects when calculating the modal gain

of plasmonic amplifiers.[25, 30] In this model, the pump distribution and modified excited-state lifetime[31] are first calculated to accurately determine the inversion. To estimate the gain of our confined SPP waveguides, we have calculated the bound modes of the equivalent planar waveguide structure with and without quenching at F_p = 48 µJ/cm². This lower power was chosen for the comparison to avoid complications arising due to saturation and bimolecular annihilation. The resulting local gain is shown in Fig. 5. The calculation predicts a modal loss of 176 dB/mm for the passive structure, a gain of 225 dB/mm for the pumped structure in the absence of quenching, and a much lower gain of 64 dB/mm when quenching is included. When the larger experimentally observed losses of 260 dB/mm are accounted for, an overall loss of 20 dB/mm can be expected. This number is in good agreement with the experimentally measured modal loss of (60 ± 10) dB/mm. However, the discrepancy suggests that even at 48 µJ/cm², bimolecular annihilation cannot be safely ignored due to the high density of excited DCM molecules.

In conclusion, we have demonstrated SPP amplification in confined plasmonic waveguides, using an optically pumped Alq₃:DCM thin film. The single mode nature of the waveguides and the observed polarization dependence clearly confirm the plasmonic nature of the observed gain. It is indeed the presence of the metal which allows the existence of *any* guided modes in our structure. Net amplification occurs at a pump fluence of F_p = 200 µJ/cm², and a mean gain of (3.4 ± 16) dB/mm was obtained via systematic measurements over a range of waveguide lengths. The highest net gain observed, shown in Fig. 3d, corresponds to 93 dB/mm and was obtained at F_p = 503 µJ/cm² for a 40 µm-long waveguide suggesting that the same geometry may support lasing via a reduction of the grating losses. The fabricated waveguides can also be used as

high contrast ratio modulators, but for indirect pumping of the laser dye previous reports have shown that stimulated emission occurs on a ~10 ps timescale, limiting operation to ~100 GHz.[32] For direct pumping of DCM, however, gain occurs on a sub-ps timescale, only limited by intramolecular relaxation.[33] Finally, CW gain remains to be demonstrated in Alq$_3$:DCM, but several strategies have recently been proposed to achieve this.[34, 35]

FIGURE CAPTIONS

Figure 1. Plasmonic waveguide structure. a) The absorbance and photoluminescence are shown for a 130 nm-thick film of Alq_3:DCM on fused silica. The weak absorbance at 515 nm corresponds to ground state absorption from DCM, while most of the remaining contribution corresponds to absorption from the host. The ASE spectrum was obtained in the variable stripe length geometry using a 250 nm-thick film. b) Optical micrograph of the plasmonic waveguides. Locations of the input and output gratings are indicated on the figure. c) Images showing a 50 μm waveguide excited under TM and TE, λ=633 nm, probe polarization. The presence of the output signal is clearly observed for electric field polarization along the waveguide (TM), consistent with the quasi-TM supported mode, while no output is observed for the perpendicular TE-polarization.

Figure 2. Passive waveguide loss. Mean output intensity observed for TM-polarization as a function of waveguide length. The standard deviation, obtained from averages over five sets of waveguides is also shown. From a simple exponential fit, a SPP propagation length of L_{exp} = (16.9 ± 0.7) μm, corresponding to a power propagation loss of α_{exp} = (258 ± 11) dB/mm is obtained. The inset shows the waveguide structure overlaid with a FEM calculation of the mode field intensity.

Figure 3. Loss compensation measurements. a) The experimental setup used to perform loss compensation measurements is shown schematically. Both probe (λ=633 nm) and pump (λ=355 nm) beams are focused onto the sample using a NUV objective.

The polarization of the probe beam is controlled using a linear polarizer (POL) and half-wave plate (HWP). A dichroic mirror (DM) is used to allow the striped shaped pump to reach the sample, but only collect the probe output. A tube lens (L_1) is used to form an image of the output and spatial selection is achieved using an iris. A second lens (L_2) is used to relay the image onto a CCD camera, a fast PMT for loss-compensation measurements, or fiber bundle. Flip mirrors (FM_1 and FM_2) are used to select the desired measurement. To reduce any residual pump light and reduce the direct fluorescence contribution to the PMT measurement 400 nm long pass (LP) and 1 nm-wide, λ=633 nm, bandpass filters (BP) are used. b) An image of the fluorescence resulting from the 67 x 10 μm rectangular probe beam taken on a 50 mm-long waveguide. Since it is not in the conjugate image plane, some weak diffraction effects due to the slit can be observed along the stripe. c) Typical loss-compensation measurement shown for a 30 μm long waveguide, taken at F_p = 200 μJ/cm^2. The figure shows the PMT output, integrated over 10^3 pulses, for TM and TE probe polarization, in the presence of the pump, and in the absence of the probe beam. Direct fluorescence can be observed for both pump–probe (TE) and pump only configurations. For the pump–probe (TM) arrangement, the DC contribution arising from the CW probe is seen. The additional signal in the presence of the pump corresponds to both the CW contribution and gain, giving a signal enhancement factor F = 3.2 ± 0.1. The data shown here are before correction for the broad PMT instrument-response function, as compared to the pump beam (see Supporting Information). Note that the small peak observed at 26 ns is an artefact resulting from PMT afterpulsing. d) The signal enhancement and fluorescence are shown, as a function of increasing pump fluence for a 40 μm-long waveguide. The fluorescence is measured in

the same geometry *via* the peak signal induced by the pump in the absence of a probe beam. The grey region corresponds to net gain. The same saturation regime is clearly observed in both cases (the lines are guides to the eye), and corresponds to the onset of bimolecular annihilation mechanisms.

Figure 4. Length dependence of the gain. Dependence of the signal enhancement as a function of waveguide length for pump fluences a) $F_p = 48$ µJ/cm^2 and b) $F_p = 200$ µJ/cm^2. The measurements are averages, obtained from five sets of waveguides. The error bars show the standard deviation, while the grey region shows the lowest and highest enhancements observed. The dashed line shows the net gain threshold which is exceeded for most measurements made at $F_p = 200$ µJ/cm^2. From the slope, which excludes the anomalous 50 µm length, and the measured passive losses we find a net gain (3.4 ± 16) dB/mm.

Figure 5. Local gain of planar structure. The figure shows a calculation of the local gain, at $F_p = 48$ µJ/cm^2, for the equivalent planar structure accounting for the spatial pump distribution, with and without quenching from the modified emitter lifetime taken into account. Because the stripe width is significantly larger than cutoff (and confirmed by FEM calculations), the gain obtained from the planar structure is not expected to differ significantly from that of the finite-width structure. The calculation highlights the importance of quenching. The modal gains, g_m, are shown in units of cm^{-1} and correspond to 225 dB/mm and 64 dB/mm in the absence and presence of quenching, respectively. If the experimentally measured passive loss is used, the calculation predicts a net loss of 20

dB/mm at this fluence, which compares favourably to the measured loss of (60 ± 10) dB/mm. In all cases, the calculation ignores any saturation or bimolecular processes within the dye medium.

SUPPORTING INFORMATION

This material is available free of charge via the Internet at http://pubs.acs.org.

ACKNOLWEDGEMENTS

METHODS

Experimental structure

The waveguides were fabricated on Corning No.1 cover glass via e-beam lithography (Raith e_LiNE) by exposing 300 nm-thick PMMA resist, coated with a conductive polymer (ESPACER 300Z) to the electron beam. The conductive polymer was then removed in DI water and the PMMA developed in a mixture of methyl isobutyl ketone and isopropanol (1:3). To obtain good propagation at the Au-glass interface and 100% yield during lift-off, the use of a low-loss sticking layer is crucial. For this, the sample was ashed for 4 minutes in a O_2 plasma and immediately transferred to a vessel saturated with (3-mercaptopropyl)trimethoxysilane vapour to form a self-assembled monolayer at the glass surface. The 21 nm gold layer was then deposited by vacuum thermal evaporation, followed by lift-off in acetone. The self-assembled monolayer ensured good adhesion and contact between the glass-Au interface.

Obtaining large grating coupling efficiencies for thin waveguides (<30 nm) was found to be extremely challenging. To achieve this, 60 nm-thick Au in and out-coupling gratings were defined using a second-step of e-beam lithography aligned onto the pre-fabricated waveguides. Finite element method calculations (COMSOL) confirmed that this geometry increased the coupling efficiency by two orders of magnitude as compared to gratings patterned directly into the waveguides. Each grating consisted of 20 ridges with a 50% duty cycle and a $\Lambda=372$ nm period chosen from numerical simulations. Note that the strong grating perturbation results in a period slightly different from the ideal phase matching condition. The 130 nm-thick Alq_3:DCM organic gain medium was deposited onto the waveguides and gratings by co-sublimation in a vacuum of 10^{-7} mbar

at a 1.5% DCM to Alq$_3$ volume ratio. After completion, the overall coupling efficiency of the structure, given by the product of the two grating efficiencies, was measured *via* the ratio of the ouput to input probe power to be 7x10^{-4}. Using this efficiency we estimate that the SPP probe irradiance corresponds to less than 200 times the incident pump irradiance.

All of the thicknesses and refractive indices used in this work were obtained using spectroscopic ellipsometry (JA Woollam VASE). The measured permittivities at the pump wavelength (λ = 355 nm) are ε_{DCM} = 3.091-0.309i, ε_{Au} = -0.625-6.214i, ε_{glass} = 2.418, while at the SPP wavelength (λ = 633 nm) they are ε_{DCM} = 2.941, ε_{Au} = -12.272-1.480i, ε_{glass} = 2.323. The exact gold thickness measured is 21.5 nm.

Mode area

Mode areas, A_m, effective indices, n_{eff}, and propagation lengths, L_{spp}, were calculated for 1 µm-wide stripes using COMSOL. Because the investigated waveguides possess a smooth field profile, several equivalent definitions of mode area can be used.[36] We define the mode area by normalizing the integrated time-averaged electromagnetic energy density (W_{av}), by its peak value W_{peak}:

$$A_m = \frac{1}{W_{peak}} \int W_{av}(\mathbf{r}) dA$$

$$W_{av}(\mathbf{r}) = \frac{1}{4} \left(\frac{d(\omega\varepsilon(\mathbf{r},\omega))}{d\omega} |E(\mathbf{r})|^2 + \mu |H(\mathbf{r})|^2 \right)$$

which is valid when the imaginary part of $\varepsilon(\omega)$ remains small compared to its real part. The mode areas quoted and used in this work can be reduced by narrowing the waveguide width, but all possess a cutoff width determined by n_{eff}.

Characterization

The experimental setup used for characterization of the waveguides is described in the text. For the passive propagation length measurements, the probe beam was aligned onto the center of the input grating, close to the start of the waveguides to maximize the coupling efficiency, but avoid scattering from the grating edge as the dominant coupling mechanism. The radiation from the out-coupling grating was then measured using a CCD camera for both probe polarizations. The TE-polarized measurement could then be subtracted from the TM-polarized measurement to remove any weak scattered light contribution as well as the dark and read noise of the CCD. The resulting images showing only the out-coupled plasmon were then integrated as a function of waveguide length.

For the active measurements, the signal corresponding to the out-coupled plasmon was spatially selected using an iris, before being directed to the PMT (Hamamatsu H9305). The signal resulting from 10^3 pump pulses (at 70 Hz) was then averaged using a 500 MHz oscilloscope in the absence of the probe beam, and for both probe polarizations. Here, the pulse to pulse energy fluctuations had a standard deviation of 20%. The difference between the TM and TE probe signals serves to remove both the scattered probe light and fluorescence contributions to the resulting data. Note that the single-electron response of the PMT gives the characteristic weak oscillations that are observed on the oscilloscope data. In Fig. 3, measurements from waveguides with visible structural defects were discarded. The low-dynamic range intrinsic to this PMT prevented us from measuring the amplification at much higher powers without entering the non-linear regime, and thus underestimating the gain. Its use, however, was necessary to amplify the weak plasmon intensity radiated from the longer gratings above the noise floor resulting from electromagnetic interference due to the laser Pockels cell.

REFERENCES

1.   Maier, S. A., *Plasmonics : fundamentals and applications*. 1st ed.; Springer: Bath ; New York, 2007; p xxiv, 223 p.

2.   Raether, H., *Surface plasmons on smooth and rough surfaces and on gratings*. Springer-Verlag: Berlin ; London, 1987.

3.   Bozhevolnyi, S. I.; Volkov, V. S.; Devaux, E.; Laluet, J.-Y.; Ebbesen, T. W. *Nature* **2006,** 440, (7083), 508-511.

4.   Kalavrouziotis, D.; Papaioannou, S.; Giannoulis, G.; Apostolopoulos, D.; Hassan, K.; Markey, L.; Weeber, J. C.; Dereux, A.; Kumar, A.; Bozhevolnyi, S. I.; Baus, M.; Karl, M.; Tekin, T.; Tsilipakos, O.; Pitilakis, A.; Kriezis, E. E.; Avramopoulos, H.; Vyrsokinos, K.; Pleros, N. *Opt. Express* **2012,** 20, (7), 7655-7662.

5.   Plotz, G. A.; Simon, H. J.; Tucciarone, J. M. *J. Opt. Soc. Am.* **1979,** 69, (3), 419-422.

6.   Berini, P.; De Leon, I. *Nat. Photon.* **2012,** 6, (1), 16-24.

7.   Gather, M. C.; Meerholz, K.; Danz, N.; Leosson, K. *Nat. Photon.* **2010,** 4, (7), 457-461.

8.   De Leon, I.; Berini, P. *Nat. Photon.* **2010,** 4, (6), 382-387.

9.   Berini, P. *Adv. Opt. Photon.* **2009,** 1, (3), 484-588.

10.   De Leon, I.; Berini, P. *Phys. Rev. B* **2011,** 83, (8), 081414.

11.   Bergman, D. J.; Stockman, M. I. *Phys. Rev. Lett.* **2003,** 90, (2), 027402.

12.   Lu, Y.-J.; Kim, J.; Chen, H.-Y.; Wu, C.; Dabidian, N.; Sanders, C. E.; Wang, C.-Y.; Lu, M.-Y.; Li, B.-H.; Qiu, X.; Chang, W.-H.; Chen, L.-J.; Shvets, G.; Shih, C.-K.; Gwo, S. *Science* **2012,** 337, (6093), 450-453.

13.   Ma, R.-M.; Oulton, R. F.; Sorger, V. J.; Bartal, G.; Zhang, X. *Nat Mater* **2011,** 10, (2), 110-113.

14.   Noginov, M. A.; Zhu, G.; Belgrave, A. M.; Bakker, R.; Shalaev, V. M.; Narimanov, E. E.; Stout, S.; Herz, E.; Suteewong, T.; Wiesner, U. *Nature* **2009,** 460, (7259), 1110-1112.

15.   Oulton, R. F.; Sorger, V. J.; Zentgraf, T.; Ma, R.-M.; Gladden, C.; Dai, L.; Bartal, G.; Zhang, X. *Nature* **2009,** 461, (7264), 629-632.

16.   Oulton, R. F.; Sorger, V. J.; Genov, D. A.; Pile, D. F. P.; Zhang, X. *Nat. Photon.* **2008,** 2, (8), 496-500.

17.   Grandidier, J.; des Francs, G. r. C.; Massenot, S. b.; Bouhelier, A.; Markey, L.; Weeber, J.-C.; Finot, C.; Dereux, A. *Nano Lett.* **2009,** 9, (8), 2935-2939.

18.   Radko, I.; Nielsen, M. G.; Albrektsen, O.; Bozhevolnyi, S. I. *Opt. Express* **2010,** 18, (18), 18633-18641.

19.   Dang, C.; Lee, J.; Breen, C.; Steckel, J. S.; Coe-Sullivan, S.; Nurmikko, A. *Nat Nano* **2012,** 7, (5), 335-339.

20.   Berggren, M.; Dodabalapur, A.; Slusher, R. E. *Appl. Phys. Lett.* **1997,** 71, (16), 2230-2232.

21.   Bulović, V.; Kozlov, V. G.; Khalfin, V. B.; Forrest, S. R. *Science* **1998,** 279, (5350), 553-555.

22.   Kena-Cohen, S.; Stavrinou, P. N.; Bradley, D. D. C.; Maier, S. A. *Appl. Phys. Lett.* **2011,** 99, (4), 041114-3.

23.   Kozlov, V. G.; Bulovic, V.; Burrows, P. E.; Baldo, M.; Khalfin, V. B.; Parthasarathy, G.; Forrest, S. R.; You, Y.; Thompson, M. E. *J. Appl. Phys.* **1998,** 84, (8), 4096-4108.

24.   Riechel, S.; Lemmer, U.; Feldmann, J.; Berleb, S.; Mückl, A. G.; Brütting, W.; Gombert, A.; Wittwer, V. *Opt. Lett.* **2001,** 26, (9), 593-595.

25.   De Leon, I.; Berini, P. *Phys. Rev. B* **2008,** 78, (16), 161401.

26.   Krasavin, A. V.; Vo, T. P.; Dickson, W.; Bolger, P. d. M.; Zayats, A. V. *Nano Lett.* **2011,** 11, (6), 2231-2235.

27.   Berini, P. *Phys. Rev. B* **2001,** 63, (12), 125417.

28.   Siegman, A. E., *Lasers*. University Science: Sausalito, Calif., 1986; p xxii, 1283 p.

29.   Powell, R. C.; Soos, Z. G. *J. Lumin.* **1975,** 11, (1–2), 1-45.

30.   Colas des Francs, G.; Bramant, P.; Grandidier, J.; Bouhelier, A.; Weeber, J. C.; Dereux, A. *Opt. Express* **2010,** 18, (16), 16327-16334.

31.   Ford, G. W.; Weber, W. H. *Physics Reports* **1984,** 113, (4), 195-287.

32.   Kallinger, C.; Riechel, S.; Holderer, O.; Lemmer, U.; Feldmann, J.; Berleb, S.; Muckl, A. G.; Brutting, W. *J. Appl. Phys.* **2002,** 91, (10), 6367-6370.

33.   Kovalenko, S. A.; Dobryakov, A. L.; Ruthmann, J.; Ernsting, N. P. *Phys. Rev. A* **1999,** 59, (3), 2369-2384.

34.   Kéna-Cohen, S.; Wiener, A.; Sivan, Y.; Stavrinou, P. N.; Bradley, D. D. C.; Horsfield, A.; Maier, S. A. *ACS Nano* **2011,** 5, (12), 9958-9965.

35.   Zhang, Y.; Forrest, S. R. *Phys. Rev. B* **2011,** 84, (24), 241301.

36.   Oulton, R. F.; Bartal, G.; Pile, D. F. P.; Zhang, X. *New Journal of Physics* **2008,** 10, (10), 105018.
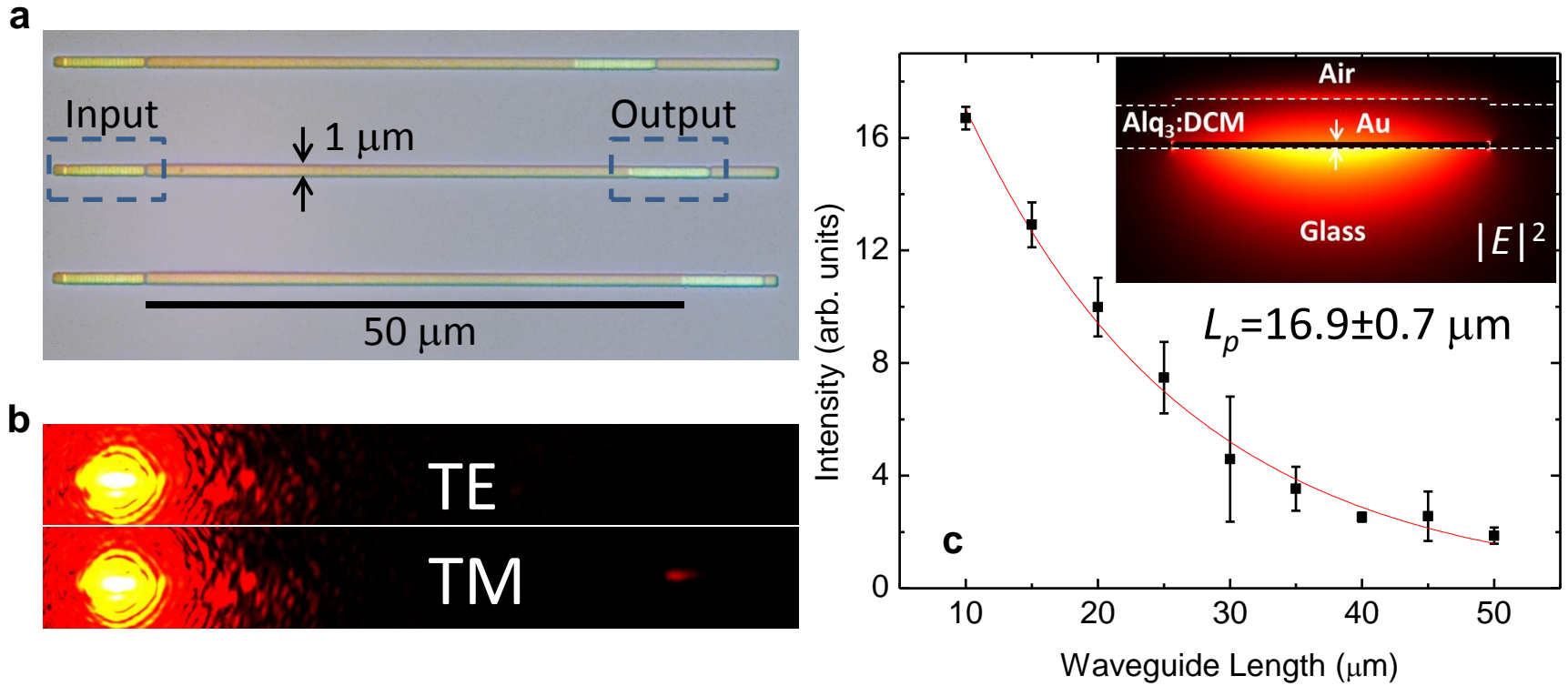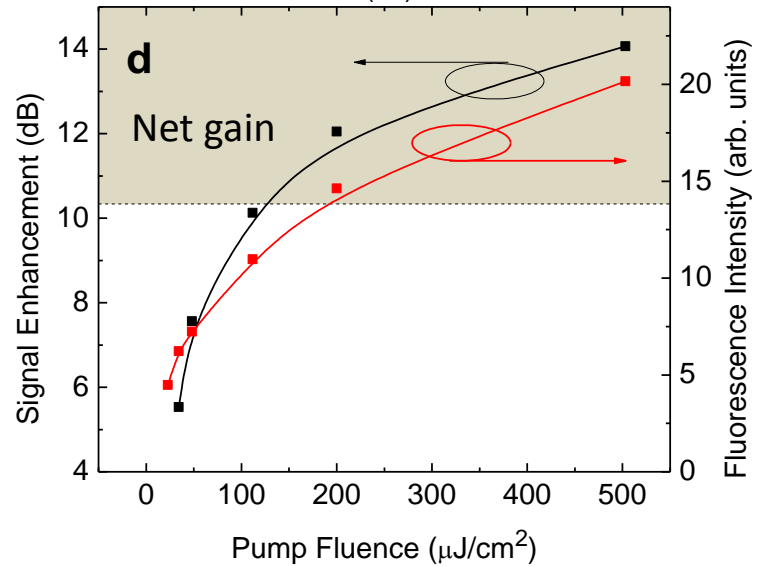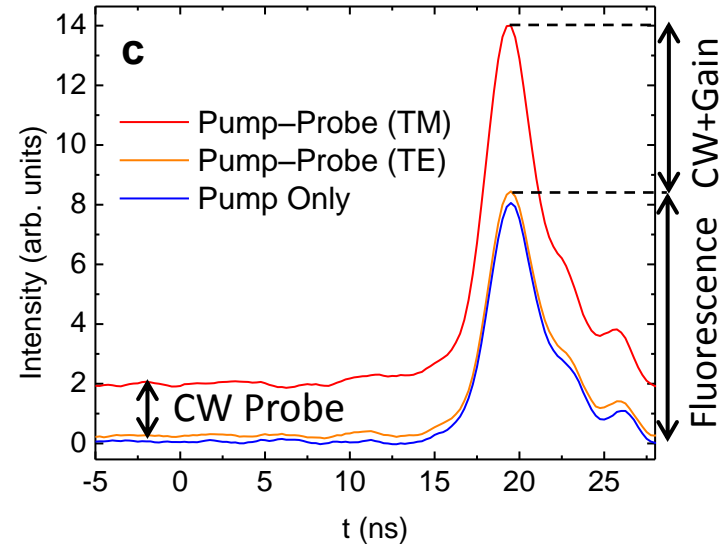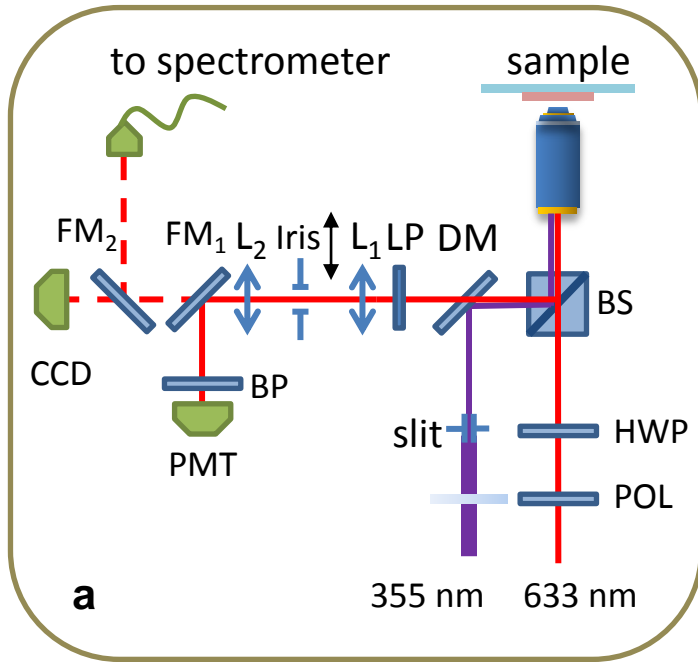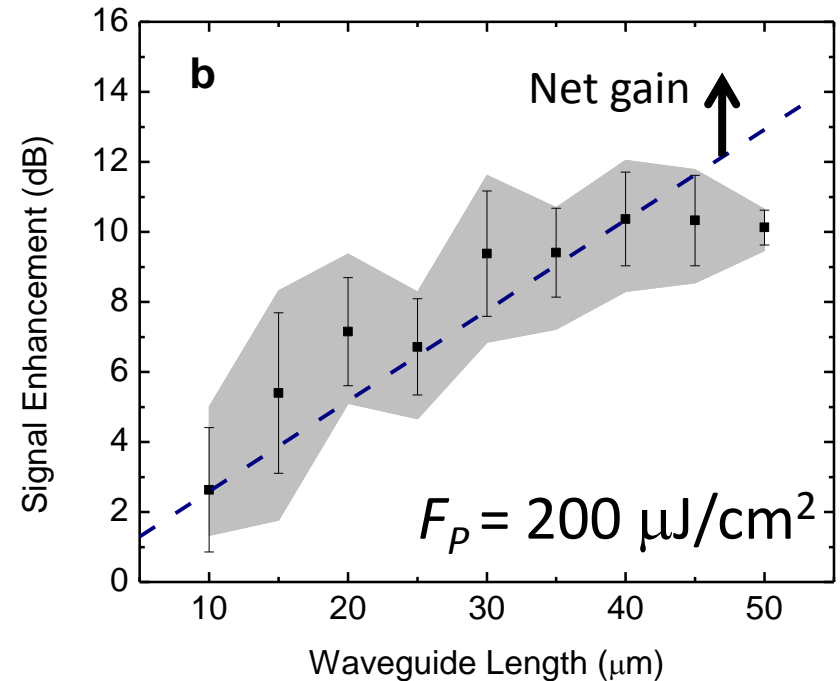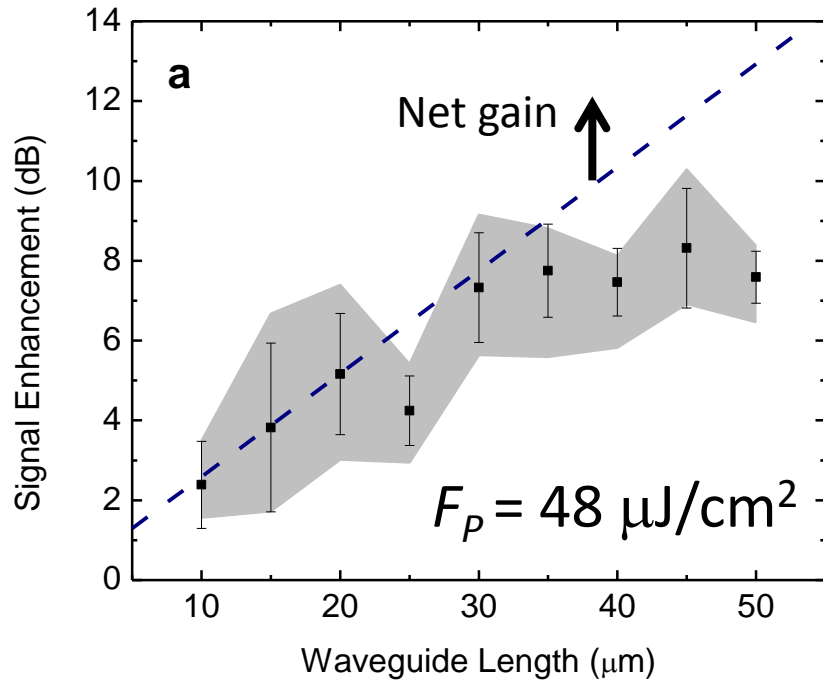
Figure 1 – Kéna-Cohen et al.

Figure 2 – Kéna-Cohen et al.

Figure 3 – Kéna-Cohen et al.

Figure 4 – Kéna-Cohen et al.